

IMPACT RESPONSE OF UHPC AND UHPFRC: EXPERIMENTAL STUDY AND NUMERICAL SIMULATION

C. PONTIROLI AND B. ERZAR*

* CEA, DAM, CEA-GRAMAT

F-46500 Gramat, FRANCE

e-mail: christophe.pontirol@cea.fr

Key words: Ballistic impact, Fiber Reinforced Concrete, Modeling, Simulation

Abstract: When a projectile hits a concrete target, several specific mechanisms are activated. Craters forms on front and rear faces of the target mainly due to shear and tensile damage. In the vicinity of the projectile nose, the concrete material is subjected to intense pressures (several hundreds of MPa), increasing its apparent ductility. Ultra-high performance concrete (UHPC) and ultra-high performance fiber reinforced concrete (UHPFRC) represent new opportunities to design protective structures. The compressive strength of these materials is commonly five times the one of standard concrete. Compared to usual concrete, the tensile behaviour of UHPC is also different: the composition is optimized to reduce the porosity and fibers can be included in the formulation (UHPFRC). To study the impact response of this kind of materials, penetration tests are conducted in Gramat on Ductal[®]FM targets using a steel projectile. Perforation experiments allowed investigating the influence of steel fibers on the impact craters and exit velocities. To simulate impact event on UHPFRC, the Pontiroli-Rouquand-Mazars (PRM) model developed in CEA-Gramat is modified based on characterization tests performed on material specimens. Hydrostatic loading, triaxial tests and shock experiments are done to study the compressive response of UHPC under high confining pressures. Quasi-static bending tests and spalling experiments are useful to investigate the tensile response and the influence of fibers on the fracture energy. This modified version of the PRM model is used to simulate the impact response of UHPC and UHPFRC.

1 INTRODUCTION

In the last decades, the possibilities offered by ultra-high performance concrete (UHPC) have been exploited by engineers and architects to design structural elements with unusual thin shapes. These families of material constitute interesting candidates for protective structures or structural elements. Indeed, the high compressive strength and the high-energy dissipation capacity due to the presence of steel fibers (UHPFRC) allow designing effective protection towards blast and ballistic threats.

Penetration tests carried out in the past 20 years have showed that increasing concrete

compressive strength resulted in decreasing penetration depths or residual velocities of the projectile after perforating concrete slabs [0-0]. It was found also that adding steel fibers was the most effective method in reducing spalling and scabbing crater dimensions of both impacted and rear faces of the targets [0-0].

Twelve years ago, CEG-DGA has conducted penetration tests on standard and ultra-high strength concrete (Ductal-FM[®]) targets using a steel penetrator [0]. For impact velocities ranging from 250 to 450 m/s, the penetration depths have been found to be 1.4 times less for a UHPFRC with a compressive

strength of 200 MPa than in a standard concrete ($f_c = 40$ MPa). Blast experiments and ballistic impact experiments with small-calibre bullet and fragment simulating projectile have been carried out on Ductal[®] targets by Cavill [0]. The ability of such concrete material to be used as protective elements has been confirmed.

Nowadays, the CEA Gramat makes constant efforts to develop and to validate models describing accurately the dynamic behaviour of concrete under extreme conditions. The numerical simulation represents a versatile tool to assess the damage and the residual load capacity of a structure subjected to blast loading or projectile impact. However, the ability of a simulation to be predictive is closely linked to the consistency of the material model. The modeling approach should take into account the main physical phenomena activated in dynamic conditions and it must be identified with reliable experimental data. This is of primary importance in the case of high amplitude loading under high strain rates, a specific loading regime associated to high velocity impact or contact detonation. Unfortunately only few experimental data under high pressure and high strain rates are available today in the literature for UHPC.

In this work, the modeling approach developed in CEA Gramat for standard concrete is first described. Then, several characterization experiments at the material scale are presented as well as corresponding calibration of PRM model for UHPC. Then, experimental results of ballistic impacts on Ductal[®] are reported and compared to similar tests carried out on a standard concrete. Finally, numerical simulations of perforation tests have been conducted and confronted to experimental data.

2 PRM MODEL

2.1 Damage model

The PRM model has been developed to simulate the behaviour of concrete under severe loading [0]. This macroscopic model,

based on the Mazars damage model proposed in 1984 [0], includes two scalar damage variables D_t and D_c that give respectively the loss of stiffness under pure tensile loading and pure compressive loading. In this generalized version of the damage model, α_t evolves between 0 and 1 (see Equation 1):

$$D = \alpha_t D_t + (1 - \alpha_t) D_c \quad (1)$$

The general 3D constitutive relations relating stress and strain tensors are given by Equation 2, where λ_0 and μ_0 are the Lamé constants defining the initial elastic stiffness of the material.

$$\sigma = (1 - D) (\lambda_0 \text{tr } \varepsilon \mathbf{I} + 2 \mu_0 \varepsilon) \quad (2)$$

A problem of mesh size dependency is often observed for damage models. In order to limit this effect, the Hillerborg regularization model has been included [12]. In this method, the energy consumed by a crack to propagate through a band of finite elements is no more dependent of the mesh size thanks to a fixed characteristic length L_c . In fact, the method consists in modifying the softening part of the stress-strain relation in order to get the same fracture energy whatever the mesh size. To do so, a new variable ω is introduced:

$$\omega = 1 \quad \text{if} \quad \varepsilon_{eq} \leq \varepsilon_p \quad (3)$$

$$\omega = \frac{\varepsilon_p}{\varepsilon_{eq}} + \left(1 - \frac{\varepsilon_p}{\varepsilon_{eq}}\right) \frac{L_c}{L_c} a(R_t) \quad \text{if} \quad \varepsilon_{eq} > \varepsilon_p \quad (4)$$

where $\varepsilon_p = \alpha_t \varepsilon_{pt} + (1 - \alpha_t) \varepsilon_{pc}$ with ε_{pt} and ε_{pc} respectively the peak strain in tension and compression. $a(R_t)$ is a corrective function dependent of the dynamic increase factor R_t . This variable ω is included into the damage formula (Eq. 5) to adapt the damage kinetic, taking into account the characteristic length L_c of the material and the finite element characteristic length L_c :

$$D_t = 1 - \frac{\varepsilon_{0t}(1 - A_t)}{\varepsilon_{eq}} - \omega A_t \exp\left(-B_t(\omega \varepsilon_{eq} - \varepsilon_{0t})\right) \quad (5)$$

In the precedent relations, ε_{0t} , ε_{0c} , A_t , A_c , B_t and B_c are material parameters and the equivalent strain is defined by Eq. 6. In this relation, X_i corresponds to the positive principal strain components.

$$\varepsilon_{eq} = \sqrt{\sum_i \langle X_i \rangle^2} \quad (6)$$

As proposed by Hillerborg [12], the characteristic length L_c is assumed to be directly linked to the fracture energy G_f and the static tensile strength f_t of the considered material:

$$L_c = \frac{E_0 G_f}{f_t^2} \quad (7)$$

For compressive loading at high strain-rates, no dynamic increase factor has been considered because the apparent increase of compressive strength is certainly due to inertial auto-confinement or non-homogeneous lateral deformation of concrete specimens during dynamic compressive tests [0], [0], [0].

2.2 Strain-rate sensitivity of tensile strength

For dynamic regime, one has to take into account the strain-rate sensitivity of concrete. Indeed, the ultimate tensile stress reached by concrete at 100 s^{-1} is usually 4 to 5 times higher than its quasi-static strength [18]. Authors are agreed to consider this effect like an intrinsic material phenomena. This aspect of the behaviour is accounted for by replacing the parameter ε_{0t}^d (initial deformation for damage in tension) by its dynamic equivalent ε_{0t}^d computed thanks to the dynamic increase factor R_t :

$$R_t = \varepsilon_{0t}^d / \varepsilon_{0t} = 1 + a_t (\dot{\varepsilon})^{b_t} \quad (8)$$

This power model has already been identified for standard concrete using quasi-static direct tension experiments and spalling tests conducted with a Hopkinson bar device [18], and with ultra-high strain-rate uniaxial deformation tests carried out with a pulsed power generator named GEPI [19]. The strain-rate sensitivity of UHPC and UHPFRC has been investigated with the same devices. Experimental results are showed on Figure 1. No differences are observed between concrete with or without fibers. Tensile strength depends essentially on cement paste behaviour. The main difference lies in the post-peak tensile behaviour. The comparison of the velocity profiles during spalling tests for UHPC and UHPFRC (with 2% steel fibers volume) allows to identify clearly the influence of fibers: the presence of fibers

induces additional residual strength and the residual velocity for this specimen is below the signal measured for a UHPC specimen which appears more brittle (see Figure 2).

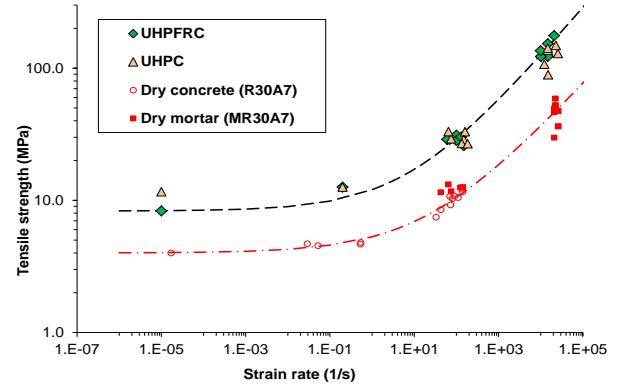


Figure 1: Strain rate effects on the dynamic tensile strength obtained on dried concrete and mortar, and on UHPC with and without fibers

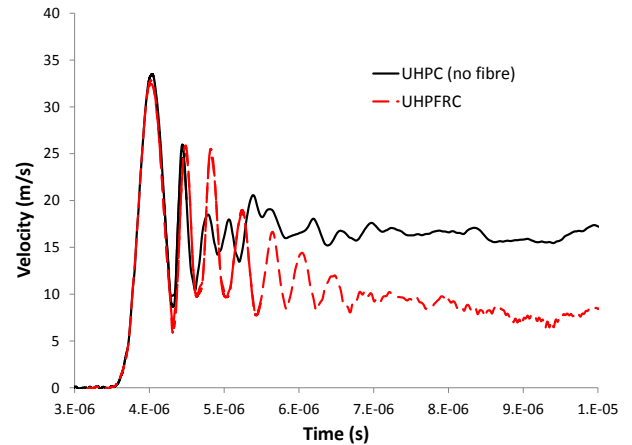


Figure 2 : Typical signals of spalling tests conducted on a UHPC and a UHPFRC specimens

2.3 Fibers influence on tensile behaviour

Besides the compressive strength, the main difference between standard concrete and UHPFRC lies in the post-peak tensile behavior (see Figure 2). Indeed, the presence of fibers offers a pronounced ductility to UHPFRC. Disseminated in the microstructure, steel fibers play a major role during the fracture process, bridging the cracks and retaining fragments. To model their influence, the fracture energy due to fibers has been introduced directly in the evolution of the tensile damage variable D_t , depending on L_f the fiber length and on the volume fraction of fibers V_f actually participating into the resistance to crack

opening. We can rewrite equations (3) and (4) by:

$$\omega = 1 \quad \text{if} \quad \varepsilon_{\text{eq}} \leq \varepsilon_p \quad (9)$$

$$\omega = \frac{\varepsilon_p}{\varepsilon_{\text{eq}}} + \left(1 - \frac{\varepsilon_p}{\varepsilon_{\text{eq}}}\right) \left[\frac{L_e}{L_c} a(R_t, V_f) + \frac{L_e}{L_f} b(V_f) \right] \quad \text{if} \quad \varepsilon_{\text{eq}} > \varepsilon_p \quad (10)$$

where $a(R_t, V_f)$ and $b(V_f)$ are functions dependent of the dynamic increase factor R_t and of the volume fraction of fibers V_f .

2.4 Plasticity and compaction modelling

The PRM damage model is efficient to simulate the dynamic response of concrete under very low confinement. However, an elastic-plastic model is more appropriate for simulating the impact of a steel projectile in a concrete slab at about 300 m/s. Indeed, in this case, pressure level of several hundreds of MPa can be observed in the vicinity of the projectile nose. Specific phenomena such as pore collapse or increase of shear strength have to be considered to model accurately the dynamic response of concrete.

To do so, the PRM damage model has been coupled with a simple plasticity model proposed by Krieg, Swenson and Taylor [20], [21].

On the one hand, in this elastic-plastic model, a parabolic relation describes the pressure-dependency of the yield stress q :

$$q = \sqrt{a_0 + a_1 p + a_2 p^2} \quad (11)$$

where p is the pressure and a_0 , a_1 and a_2 are material parameters. q is the yield stress in the sense of Von Mises plasticity:

$$q = \sqrt{\frac{3}{2} \bar{\sigma} : \bar{\sigma}} \quad (12)$$

$\bar{\sigma}$ being the deviatoric stress tensor defined as $\bar{\sigma} = \bar{\sigma} + p \cdot \bar{1}$. The increase of q with pressure can be limited by a saturation value q_{max} . This is particularly important for standard concrete which presents a saturation value linked to its water saturation level [22], [23].

On the other hand, the pore-collapse phenomenon occurring at high pressure is described by a piecewise-linear compaction curve. The elastic behaviour becomes more and more non-linear up to the full

consolidation of concrete: at this point, the pore collapse phenomenon is achieved and the material is considered fully compacted.

To identified PRM material parameters, two kinds of experiments have been carried out on the UHPC with the load cell of CEA Gramat (Figure 3a). The first test is dedicated to the determination of the compaction curve: a hydrostatic experiment is conducted by increasing the fluid pressure p_f in the load cell (Figure 3b). This test has been used to identify the response of UHPC (pressure vs volumetric strain) up to nearly 1 GPa (Figure 4a). It should be noted that at 900 MPa, only 6% of volumetric strain is observed. This value, very low in comparison to a standard concrete, is the consequence of the optimization of the composition to fill the pores at every scale.

The second type of experiment is the triaxial test. It begins with a hydrostatic loading due to fluid pressure. Then, an axial loading is applied to increase the deviatoric stress in the concrete specimen. Four tests with increasing fluid pressure of $p_f = 200, 300, 400$ and 600 MPa have been conducted. The Figure 4b presents the results through q - p plot where the stress difference q and the average stress p are defined by:

$$q = \sigma_z - p_f$$

$$p = \frac{1}{3} (\sigma_z + 2 p_f)$$

where σ_z is the axial compression stress amplitude, counted as positive. It can be pointed out that q corresponds to the equivalent stress defined by Von Mises and Tresca in this particular case.

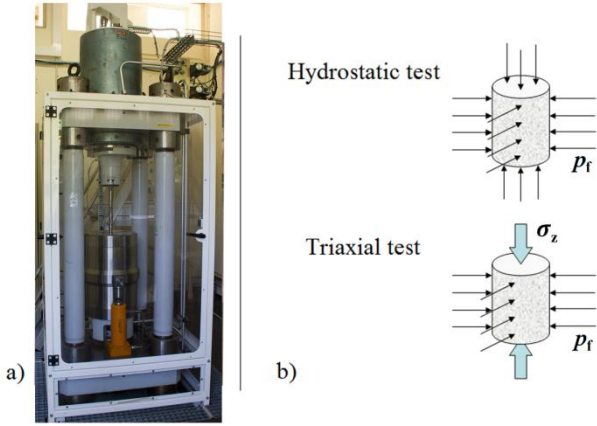


Figure 3. (a) High capacity load cell in CEA Gramat and (b) experiments in confined compression conducted on UHPC specimens.

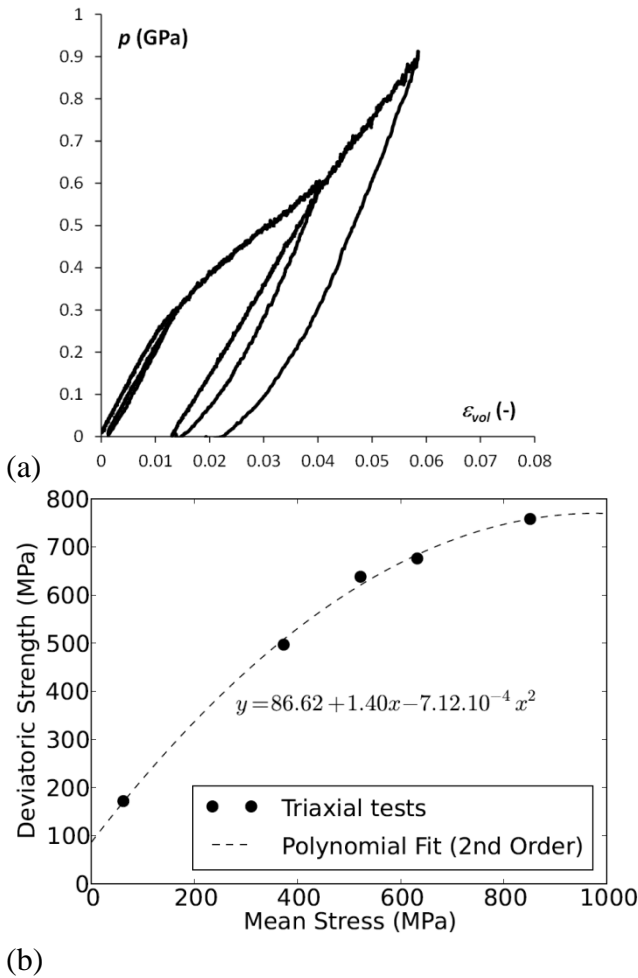


Figure 4. Compaction curve of UHPC (without steel fibers) obtained through a purely hydrostatic test (a), and shear failure from different triaxial tests (b)

Even if the data gathered in the quasi-static experimental configuration are necessary to assess the pressure dependency of the deviatoric strength, the characterization is limited to pressures lower than 1 GPa.

However, the stress level reached locally in a concrete target near an explosive charge or in front of a penetrating fragment may be notably higher. Consequently, the dataset has been completed in the shock regime response up to 6 GPa by means of plate impact experiments [24].

These plasticity and compaction models are complementary to the PRM damage model. The fully coupled PRM model includes all these mechanisms with a perfect continuity between the compressive damage definition and the plasticity model. It has been implemented in a classical finite elements code (Abaqus/Explicit [25]) through a VUMAT subroutine. This choice allows conducting numerical simulations from the material scale up to the structural response.

3 PERFORATION EXPERIMENTS

To translate the experimental results from the material scale to the structure scale, perforation tests have been performed at CEA-Gramat on UHPC and UHPRFC concrete (Ductal[®]FM with a compressive strength of 180-200 MPa). A 98 mm caliber gas gun has been used for impact tests (Figure 5).

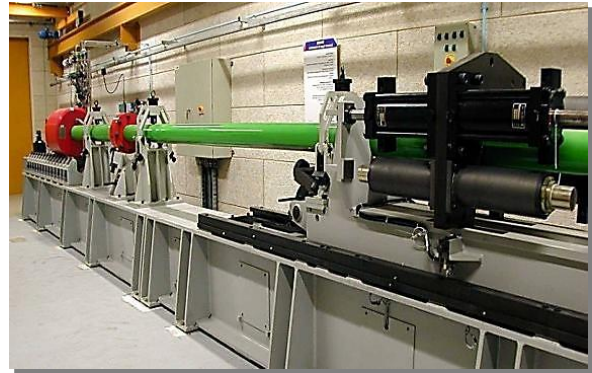


Figure 5. Gas launcher

The conical nose projectile has a total length of 240 mm and 40 mm in diameter. The total mass is 1.6 kg. The body is made of high strength steel 35NCD16. The targets were 150 cm squared slabs of concrete. The thickness was either 10 and 30 cm. As concrete is a highly fibered material (2% steel fiber volume ratio), no additional rebar was needed, only single rebar were added closest to the target

boundaries. The experiments considered different impact velocities and angles of obliquity 0°, 15 and 30°. Yaw and pitch angles have been verified to be negligible.

Figure 6 shows projectile and experiment configuration for impact tests.

Table 1 Table 2 give perforation results in terms of exit velocity function on impact velocity, obliquity angle and concrete thickness. Fibers affect exit velocities especially for thick slabs. Figure 7 allows comparing crater dimensions on the front face with or without fiber. Brittle fracture mode can be observed on concrete without fiber while with fiber cratering is driven by ductile behaviour.



Figure 6. Projectile and experiment configuration

Table 1 : Experimental results for 10 cm in thickness

Obliquity angle	0		15°		30°	
	no fiber	fiber	no fiber	fiber	no fiber	fiber
V_{impact} (m/s)	320	331,5	300	321,7	331,2	345
V_{exit} (m/s)	236	238	215	204	234	226,5

Table 2 : Experimental results for 30 cm thickness

Obliquity angle	0		30°	
	no fiber	fiber	no fiber	fiber
V_{impact} (m/s)	700	702/703	716	702/704
V_{exit} (m/s)	-	368/357	364	168/136



Figure 7 : Cratering with or without fiber

4. NUMERICAL SIMULATIONS

The capabilities of the PRM model have been analyzed with ABAQUS/explicit code (v2018) by the restitution of experiments conducted on projectile perforation in concrete structures.

We have used 3D solid finite elements and the projectile has been assumed to behave as a rigid body (no deformation has been observed on projectile after experimental tests and we neglect slight erosion induced on the projectile nose). For concrete without fiber, PRM model has been used. For UHPFRC two modeling approaches have been tested:

- a macroscopic approach using PRM model by considering an homogenized material,
- a mesoscopic approach with a separate discrete modeling for cement paste and fiber. 3D solid finite elements are used for mortar and steel fibers are introduced in volumic model using embedded two-node beam finite elements.

Some technical problems and limitations with Abaqus/Explicit have obligated to used mesoscopic approach only for perforation target with 10 cm in thickness. Furthermore, to reduce finite element model size only the projectile penetration zone is modeling with this approach (a cylindrical zone with 30 cm in diameter and 10 cm in thickness). From the fiber content V_f and the geometrical properties of both the steel fiber L_f and concrete specimen, a cloud of fibers is generated using uniform random distribution. Single segments are sufficient for generating straight fibers. Due to the cast and target thickness, fiber orientation is not random but has a bias

towards a preferential direction parallel to the target surface. For target with 10 cm in thickness, algorithm code has generated about 1.8 millions beam elements for modeling steel fibers. About 7 millions 3D finite elements are used to discretize concrete material.

PRM model is chosen for plain concrete and a one-dimensional elastoplastic constitutive model is using for steel fiber. Using embedded method for steel fiber, a perfect adherence is assumed with concrete 3D finite element.

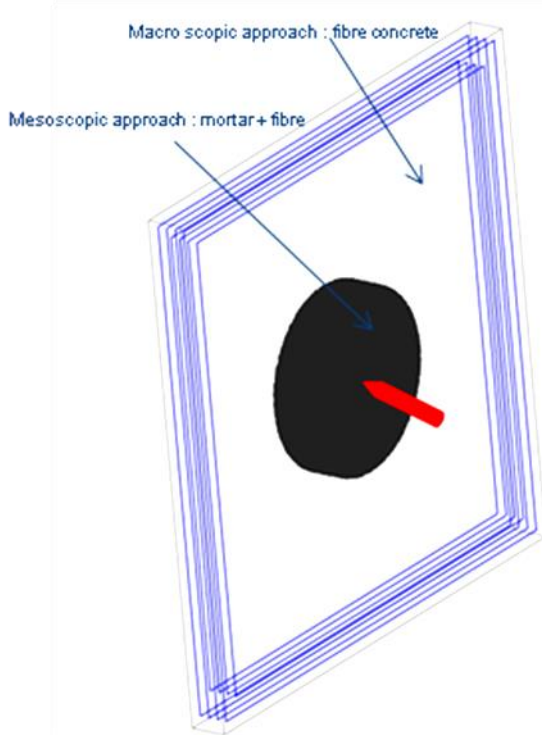


Figure 8 : FE model of UHPFRC target under impact

Perforation simulations have been performed with Abaqus/Explicit code. Comparisons between experimental and numerical results are presented in Table 3 and Table 4 in terms of exit velocities obtained for 10 and 30 cm thickness targets. As said previously, mesoscopic approach could be only applied for thin wall.

For concrete with 10 cm in thickness, a good correlation has been obtained between experimental tests and the two numerical approaches proposed in this study. Figure 9 shows numerical damage on front and rear UHPC target faces during projectile perforation simulation.

The most significant difference between

numerical and experimental result is observed for the incident impact on thick UHPFRC slab. Further investigations and mesoscopic simulations had to be performed to understand this gap.

Table 3 : Experimental/numerical comparisons for 10 cm in thickness

Obliquity angle	0		15°		30°	
	no fiber	fiber	no fiber	fiber	no fiber	fiber
V_{impact} (m/s)	320	331,5	300	321,7	331,2	345
$V_{\text{exit}}^{\text{exp}}$ (m/s)	236	238	215	204	234	226,5
Macro. $V_{\text{exit}}^{\text{num}}$ (m/s)	232	230	213	218	240	228
Meso. $V_{\text{exit}}^{\text{num}}$ (m/s)	-	227	-	217	-	229

Table 4 : Experimental/numerical comparisons for 30 cm thickness

Obliquity angle	0		30°	
	no fiber	fiber	no fiber	fiber
V_{impact} (m/s)	700	702/703	716	702/704
$V_{\text{exit}}^{\text{exp}}$ (m/s)	-	368/357	364	168/136
Macro. $V_{\text{exit}}^{\text{num}}$ (m/s)	350	324	346	241

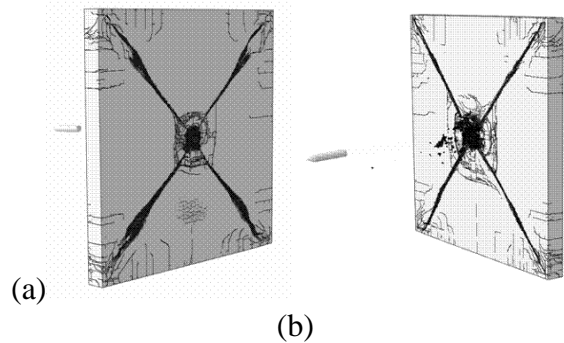


Figure 9 : Front (a) and rear (b) UHPC target faces during penetration obtained by numerical simulation

Damage patterns can be also assessed and

compared with experimental results. Figure 10 and Figure 11 compare experimental cracks zones and numerical damage patterns for normal incidence perforation and with an obliquity angle of 30° for impact on UHPC target. Crater dimensions due to scabbing spalling phenomena on front and rear faces of concrete slabs are similar between experimental and numerical results. PRM model is able to reproduce correctly the brittle behaviour of plain concrete.

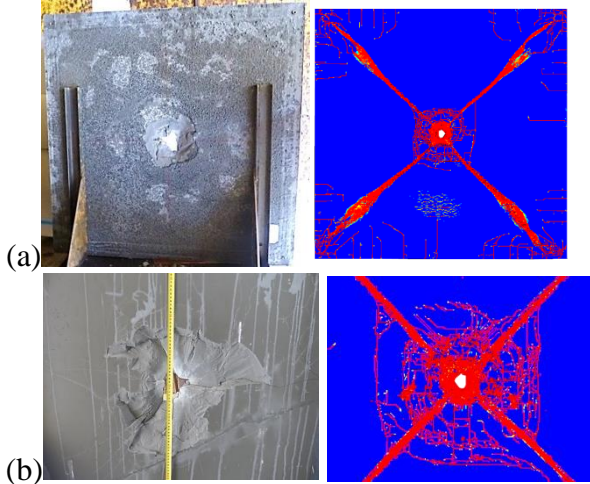


Figure 10 : Comparison of damage pattern on front (a) and rear (b) faces for UHPC normal perforation with 320 m/s impact velocity

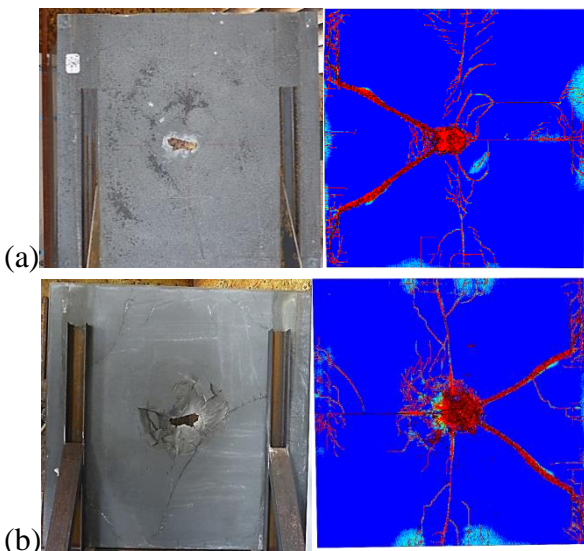


Figure 11 : Comparison of damage pattern on front (a) and rear (b) faces for UHPC perforation with AOI = 30° and 331.2 m/s impact velocity

Figure 12 shows comparisons between experimental and, macroscopic and mesoscopic numerical approaches for UHPFRC normal incidence perforation.

Numerical simulations using PRM model with homogenized behaviour (concrete + steel fibers) or using separate discretization of steel fibers and cement paste give together similar damage pattern compare to experimental facies. Numerical model can reproduce correctly the ductility behaviour of UHPFRC due to steel fibers presence.

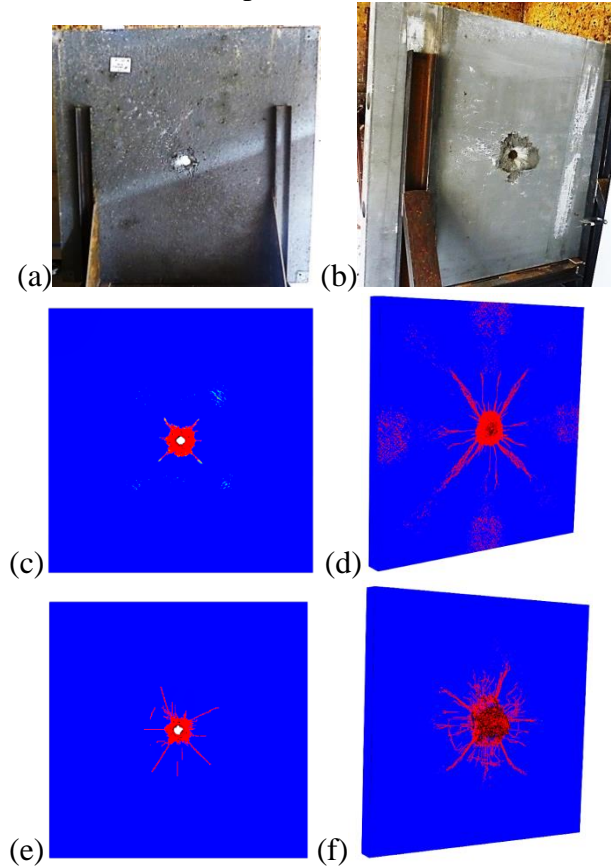


Figure 12 : Comparison of damage pattern on front (a), (c), (e) and rear (b), (d), (f) faces for UHPFRC normal perforation with 331.5 m/s impact velocity – using macroscopic approach (c), (d) and mesoscopic approach (e), (f)

Figure 13 give comparison between experiment and simulation of bridge effect due to fibers. Fibers prevent the crack opening on cement paste. Erosion method is used on numerical simulations to remove 3D finite elements with large deformations which could be slowed down or sometimes stopped calculation.

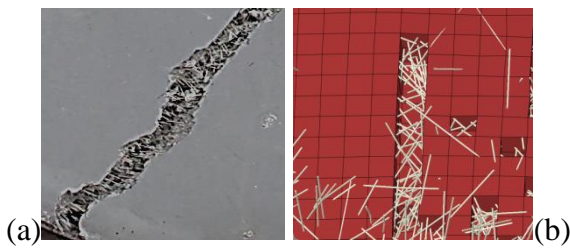


Figure 13 : Experimental (a) and numerical (b) comparison of fiber effect to bridge cracks

12 CONCLUSIONS

The design of new protective structures exposed to blast loads or high velocity impact using UHPFRC can be undertaken through numerical simulations. However, the constitutive and damage models have to be accurate and validated with reliable data. Thus, considering the relatively recent knowledge concerning mechanical response of this class of materials, extensive mechanical characterization is still necessary.

In this work, quasi-static and dynamic mechanical tests have been conducted on UHPC and UHPFRC to identify the main characteristics of the UHPFRC response in tension and in confined compression. Then, a new material parameters dataset has been calibrated for fully coupled PRM model. This sophisticated concrete model consists in a phenomenological modeling approach including the main mechanisms activated under high strain rate and high confining pressure, coupling damage to plasticity and compaction. The influence of steel fibers disseminated in the concrete has been included in the model: the damage kinetic has been modified to improve the description of the fiber influence on the dynamic tensile fracture of UHPFRC.

The modeling approach has been validated step by step using characterization data. The final evaluation of the PRM model consists in simulating perforation problems in UHPC and UHPFRC targets. Two numerical approaches for modeling cement paste and steel fibers have been proposed, one using the macroscopic and homogenized PRM model, the other using a discrete representation of fibers independently of cement paste material. Projectile residual velocities and damage

patterns in the concrete block allowed comparing qualitatively the numerical predictions with experimental results. First perforation simulations show the capacities of the two numerical methods to reproduce the UHPC brittle and the UHPFRC ductile behaviours. Further works and others numerical comparisons with experimental tests, as closest detonation near UHPFRC slabs, had to be continued to validate and improve PRM model.

ACKNOWLEDGEMENTS

This work was supported by DGA (French General Delegation for Armament, Ministry of Defence). The authors are also grateful to P. Forquin (3SR Laboratory, Grenoble Alpes University, France) for his technical contribution to this project.

REFERENCES

- [1] Hanchak SJ, Forrestal MJ, Young ER, Ehrgott JQ. 1992. Perforation of concrete slab with 48 MPa (7 ksi) and 140 MPa (20 ksi) unconfined compressive strength. *Int. J. Impact Eng.* 12(1), 1-7.
- [2] Dancygier AN, Yankelevsky DZ, Jaegermann C. 2007. Response of high performance concrete plates to impact of non-deforming projectiles. *Int. J. Impact Eng.* 34, 1768-1779.
- [3] O'Neil EF, Neeley BD, Cargile JD. 1999. Tensile properties of very-high-strength concrete for penetration-resistant structures. *Shock Vib.* 6, 237-245.
- [4] Dancygier AN, Yankelevsky DZ. 1996. High strength concrete response to hard projectile impact. *Int J Impact Eng.* 18(6), 583-99.
- [5] Dancygier AN. 1998. Rear face damage of normal and high-strength concrete elements caused by hard projectile impact. *ACI Struct. J* 5(3), 291-304.
- [6] Zhang MH, Shim VPW, Lu G, Chew CW. 2005. Resistance of high-strength concrete to projectile impact. *Int. J. Impact Eng.* 31(7), 825-41.
- [7] H. Wu, Q. Fang, X.W. Chen, Z.M. Gong and J.Z. Liu. 2015. Projectile penetration

- of ultra-high performance cement based composites at 510-1320 m/s. *Construction and Building Materials* 74, 188-200.
- [8] Buzaud E., Laurensou R., Sigeaud J.M. 2004. A computational technique for penetration of concrete targets by oblique impacts of deformable projectiles. 21st International Symposium on Ballistics, Adelaide, Australia.
- [9] Cavill B., Rebentrost M., Perry V. 2006. Ductal® - An ultra-high-performance material for resistance to blasts and impacts. Specialty Conference on Disaster Mitigation, Calgary, Canada.
- [10] Pontiroli C., Rouquand A, Mazars J. 2010. Predicting concrete behaviour from quasi-static loading to hypervelocity impact: an overview of the PRM model. *European Jour. of Environmental and Civil Engineering* 14, 703-727.
- [11] Mazars, J. 1986. A description of micro and macro scale damage of concrete structures. *Engineering Fracture Mechanics* 25, 729-737.
- [12] A. Hillerborg, M. Modeer, P.E. Petersson. 1976. Analysis of crack formation and growth in concrete beams of fracture mechanics and finite elements. *Cement and Concrete Research* 6, 773-782.
- [15] Janach W. 1976. The role of buckling in brittle failure of rocks under rapid compression. *International Journal of Rocks Mechanics and Mining Sciences & Geomechanics Abstracts* 13 (6), 177-186.
- [16] Li Q.M., Meng H. 2003. About the dynamic strength enhancement of concrete-like materials in a split Hopkinson pressure bar test. *International Jour. Solids and Structures* 40, 343-360.
- [17] Schwer L. 2009. Strain rate induced strength enhancement in concrete: Much ado about nothing? 7th European LS-DYNA Conference.
- [18] Erzar B., Forquin P. 2010. An Experimental Method to Determine the Tensile Strength of Concrete at High Rates of Strain. *Experimental Mechanics* 50, 941-955.
- [19] Erzar B., Buzaud E., Chanal P.Y. 2013. Dynamic tensile fracture of mortar at ultra-high strain-rates. *J. Appl. Phys.* 114, 244901.
- [20] Krieg, R.D. 1978. A simple constitutive description for soils and crushable foams. Sandia National Laboratories report, SC-DR-72-0833, Albuquerque, New Mexico.
- [21] Swenson D.V., Taylor L.M. 1983. A finite element model for the analysis of tailored pulse simulation of boreholes. *Int. J. Numer. Anal. Meth. Geomech.* 7, 469-484.
- [22] Vu X.H. 2007. Caractérisation expérimentale du béton sous fort confinement : influence du degré de saturation et du rapport eau/ciment. Thèse de doctorat, Laboratoire 3S-R, Grenoble.
- [23] Vu X.H., Malecot Y., Daudeville L., Buzaud E. 2008. Experimental analysis of concrete behavior under high confinement: Effect of the saturation ratio. *International Journal of Solids and Structures* (doi: 10.1016/j.ijsolstr.2008.10.015)
- [24] Erzar B., Pontiroli C., Buzaud E. 2016. Shock characterization of an ultra-high strength concrete. *European Physical Journal Special Topics.* (doi: 10.1140/epjst/e2016-02637-4)
- [25] Abaqus Manual. 2018, Dassault Systèmes.